HYDROMAGNETIC FLOW AND HEAT TRANSFER OVER A BIDIRECTIONAL STRETCHING SURFACE IN A POROUS MEDIUM

by

Iftikhar AHMAD [a*], ***Manzoor AHMED*** [a], ***Zaheer ABBAS*** [b], ***and Muhammad SAJID*** [c]

[a] Department of Mathematics, Azad Kashmir University, Muzaffarabad, Pakistan
[b] Department of Mathematics, Faculty of Basic and Applied Sciences, Islamabad, Pakistan
[c] Theoretical Plasma Physics Division, PINSTECH, Nilore, Islamabad, Pakistan

Original scientific paper
UDC: 532.546:536.24:537.84
DOI: 10.2298/TSCI100926006A

In this study, we present a steady 3-D magnetohydrodynamic flow and heat transfer characteristics of a viscous fluid due to a bidirectional stretching sheet in a porous medium. The heat transfer analysis has been carried out for two heating processes namely (1) the prescribed surface temperature and (2) prescribed surface heat flux. In addition the heat transfer rate varies along the surface. The similarity solution of the governing boundary layer partial differential equations is developed by employing homotopy analysis method. The quantities of interest are velocity, temperature, skin-friction, and wall heat flux. The results obtained are presented through graphs and tabular data. It is observed that both velocity and boundary layer thickness decreases by increasing the porosity and magnetic field. This shows that application of magnetic and porous medium cause a control on the boundary layer thickness. Moreover, the results are also compared with the existing values in the literature and found in excellent agreement

Key words: *viscous fluid, magnetohydrodinamics flow, porous medium, variable surface temperature, internal heat generation, homotopy analysis method*

Introduction

The boundary layer flows and heat transfer of Newtonian fluids over a continuously stretching surface have many important applications in several engineering and industrial processes. Examples include the extrusion of a polymer sheets from a die or in the drawing of plastic films, the boundary layer along a liquid film condensation process, the cooling process of metallic plate in a cooling bath, cooling of continuous strips, aerodynamic extrusion of plastic sheets, crystal growing, and many others. After the pioneering work of Sakiadis [1, 2] the boundary layer flow induced by a stretching sheet has been studied by many researchers [3-13] and for Newtonian fluids under various aspects of the flow phenomenon.

* Corresponding author; e-mail: aaiftikhar@yahoo.com

All the above mentioned studies were limited to 2-D boundary layer problems for linear stretching surface in one direction. Wang [14] discussed 3-D flow of a viscous fluid due to the stretching of the elastic surface in two lateral directions. He applied the direct numerical integration to the resulting boundary value problem. Laha *et al*. [15] studied the heat transfer analysis of the 3-D flow of a viscous fluid caused by a stretching sheet with uniform tension in two horizontal directions by considering a constant temperature and uniform heat flux. Recently, Ariel [16] presented the generalized 3-D flow due to a stretching sheet and demonstrated that the resulting problem admits a solution in term of series of exponentially decaying functions. Recently, Liu *et al*. [17] investigated the heat transfer characteristics over a bidirectional stretching sheet with variable thermal conditions in the presence of a temperature-dependent internal heat source (or sink). Very recently, Abdullah [18] discussed the analytical solution of heat and mass transfer for 3-D flow over a permeable stretching surface by considering the effects of chemical reaction, internal heat, Dufour-Soret and Hall current.

In all previous work done by the researchers [1-18], they did not consider the effects of applied magnetic filed over a bidirectional stretching surface in a porous medium. Therefore, the main purpose of the present paper is to extend the problem of Liu *et al*. [17] in three directions namely (1) to consider the effects of an applied magnetic filed under the low magnetic Reynolds number approximation (2) to analyze the flow in a porous medium, and (3) to provide an analytic solution to the non-linear problem using homotopy analysis method (HAM). The analytic series solution is developed using HAM [19, 20]. This technique has already been successfully applied to various problems [21-28] . To the best of our knowledge, no such analytical solution has previously been reported for magnetohydrodinamics (MHD) flow of a viscous fluid over a bidirectional stretching surface in a porous medium.

Basic equations

Consider the steady 3-D boundary layer flow of an incompressible hydromagnetic viscous fluid in a porous medium due to a stretching surface in a plane at $z = 0$. The surface is stretched uniformly in both horizontal directions with velocity components ax and by in x- and y-directions, respectively. A uniform magnetic field $\vec{B}_0$ is applied parallel to z-direction. The effects of the induced magnetic field is neglected, which is a valid assumption on a laboratory scale under the assumption of low magnetic Reynolds number. It is also assumed that the external electric field is zero. Under the usual boundary layer approximations the MHD flow of a viscous fluid is governed by equations:

$$\frac{\partial u}{\partial x}+\frac{\partial v}{\partial y}+\frac{\partial w}{\partial z}=0 \tag{1}$$

$$u\frac{\partial u}{\partial x}+v\frac{\partial u}{\partial y}+w\frac{\partial u}{\partial z}=\nu\frac{\partial^2 u}{\partial z^2}-\frac{\sigma B_0^2}{\rho}u-\frac{\phi_1\nu}{k}u \tag{2}$$

$$u\frac{\partial v}{\partial x}+v\frac{\partial v}{\partial y}+w\frac{\partial v}{\partial z}=\nu\frac{\partial^2 v}{\partial z^2}-\frac{\sigma B_0^2}{\rho}v-\frac{\phi_1\nu}{k}v \tag{3}$$

$$u\frac{\partial T}{\partial x}+v\frac{\partial T}{\partial y}+w\frac{\partial T}{\partial z}=k_1\frac{\partial^2 T}{\partial z^2}-\frac{q}{\rho c_p}(T-T_\infty) \tag{4}$$

where u, v, and w are the velocity components in the x-, y- and z-directions, respectively, ρ is the fluid density, ν – the kinematic viscosity, σ – the electrical conductivity of the fluid, ϕ_1 – the porosity, k – the permeability of the porous medium, T – the temperature, c_p – the specific heat capacity at constant pressure of the fluid, k_1 – the thermal diffusivity of the fluid, and the last term in eq. (4) represents a temperature-dependent heat source ($q > 0$) or sink ($q < 0$). In eqs. (2) and (3) the pressure gradient is neglected because it is assumed that flow is caused only by the stretching of the sheet. This assumption is also consistent with the conditions at the free stream. Furthermore, the Darcy's law has been employed for obtaining the governing equations in a porous medium.

The appropriate boundary conditions of the problem are given by:

$$u=ax,\quad v=by,\quad w=0 \quad \text{at} \quad z=0 \quad \text{and} \quad u\to 0,\quad v\to 0 \quad \text{as} \quad z\to\infty \tag{5}$$

where $a > 0$ and $b > 0$ are constant stretching rates with dimension [s^{-1}] in x- and y-directions, respectively.

For temperature we have two sets of boundary conditions:

Case a: Prescribed surface temperature (PST)

$$T=T_w(x,y)=T_\infty+Ax^r y^s \quad \text{at} \quad z=0 \quad \text{and} \quad T\to T_\infty \quad \text{as} \quad y\to\infty \tag{6}$$

Case b: Prescribed surface heat flux (PHF)

$$-\lambda\frac{\partial T}{\partial z}=Bx^r y^s \quad \text{at} \quad z=0 \quad \text{and} \quad T\to T_\infty \quad \text{as} \quad y\to\infty \tag{7}$$

where λ is the thermal conductivity of the fluid, T_∞ – the constant temperature outside the thermal boundary layer, and A and B are positive constants. The power indices r and s determine how the temperature or the heat flux at the sheet varies in the xy-plane.

Defining the similarity transformations:

$$\begin{gathered} u=axf'(\eta),\ v=byg'(\eta),\ w=-\sqrt{a\nu}[f(\eta)+g(\eta)],\quad \eta=\sqrt{\frac{a}{\nu}}z \\ \text{PST: } \theta(\eta)=\frac{T(x,y,z)-T_\infty}{T_w(x,y)-T_\infty},\quad \text{PHF: } T(x,y,z)-T_\infty=\frac{B}{\lambda}\sqrt{\frac{\nu}{a}}x^r y^s\phi(\eta) \end{gathered} \tag{8}$$

where primes denote the differentiation with respect to η. Substituting eq. (8) into eq. (2), it is satisfied automatically and from eqs. (3) and (4) become:

$$f'''+(f+g)f''-f'^2-(\varepsilon+M^2)f'=0 \tag{9}$$

$$g'''+(f+g)g''-g'^2-(\varepsilon+M^2)g'=0 \tag{10}$$

$$\theta''+\Pr(f+g)\theta'+\Pr(\beta-rf'-sg')\theta=0 \tag{11}$$

$$\phi'' + \Pr(f+g)\phi' + \Pr(\beta - rf' - sg')\phi = 0 \tag{12}$$

and the boundary conditions (5)-(7) give:

$$\begin{gathered} f(0)=0, \quad g(0)=0, \quad f'(0)=1, \quad g'(0)=\frac{b}{a}=\alpha, \quad \theta(0)=-1, \\ \phi'(0)=-1, \quad f'(\infty)=0, \quad g'(\infty)=0, \quad \theta(\infty)=0, \quad \phi(\infty)=0 \end{gathered} \tag{13}$$

and $\alpha = b/a$ is the stretching ratio. Here $\varepsilon = \phi_1/\rho ak$ is the dimensionless porosity parameter, $M^2 = \sigma B_0^2/a\rho$ – the magnetic parameter, $\Pr = \nu/k_1$ – the Prandtl number, and $\beta = q/\rho ac_p$ – the internal heat parameter.

The physical quantities of interest are the skin friction coefficients along the x- and y-directions, C_{fx} and C_{fy}, which are defined as:

$$C_{fx} = \frac{\tau_{wx}}{\rho u_w^2}, \quad C_{fy} = \frac{\tau_{wy}}{\rho u_w^2} \tag{14}$$

where τ_{wx} and τ_{wy} are the wall shear stress along the x- and y-directions, respectively. In dimensionless form we get:

$$\mathrm{Re}_x^{1/2} C_{fx} = f''(0), \quad \mathrm{Re}_x^{1/2} C_{fy} = \frac{v_w}{u_w} g''(0) \tag{15}$$

where $\mathrm{Re}_x = u_w x/\nu$ is the local Reynolds number.

Homotopy analysis solution

For the analytical solution, eqs. (9) to (13) are solved by employing HAM. Therefore, the velocity and temperature distributions $f(\eta)$, $g(\eta)$, $\theta(\eta)$, and $\phi(\eta)$ can be expressed by the set of base functions:

$$\eta^k \exp(-n\eta) \,|\, k \geq 0, n \geq 0 \tag{16}$$

with

$$f(\eta) = a_{0,0}^0 + \sum_{n=0}^{\infty}\sum_{k=0}^{\infty} a_{m,n}^k \eta^k \exp(-n\eta) \tag{17}$$

$$g(\eta) = b_{0,0}^0 + \sum_{n=0}^{\infty}\sum_{k=0}^{\infty} b_{m,n}^k \eta^k \exp(-n\eta) \tag{18}$$

$$\theta(\eta) = \sum_{n=0}^{\infty}\sum_{k=0}^{\infty} c_{m,n}^k \eta^k \exp(-n\eta) \tag{19}$$

$$\phi(\eta) = \sum_{n=0}^{\infty}\sum_{k=0}^{\infty} d_{m,n}^k \eta^k \exp(-n\eta) \tag{20}$$

and $a_{m,n}^k$, $b_{m,n}^k$, $c_{m,n}^k$, and $d_{m,n}^k$ are coefficients. Based on the rule of solution expressions and the boundary conditions (13), the initial approximations $f_0(\eta)$, $g_0(\eta)$, $\theta_0(\eta)$, and $\phi_0(\eta)$ of the functions $f(\eta)$, $g(\eta)$, $\theta(\eta)$, and $\phi(\eta)$ are:

$$f_0(\eta) = 1 - \exp(-\eta) \tag{21}$$

$$g_0(\eta) = \alpha[1 + \exp(-\eta)] \tag{22}$$

$$\theta_0(\eta) = \exp(-\eta) \tag{23}$$

$$\phi_0(\eta) = \exp(-\eta) \tag{24}$$

and the auxiliary linear operators are:

$$L_1(f) = \frac{\mathrm{d}^3 f}{\mathrm{d}\eta^3} - \frac{\mathrm{d}f}{\mathrm{d}\eta} \tag{25}$$

$$L_2(f) = \frac{\mathrm{d}^2 f}{\mathrm{d}\eta^2} - f \tag{26}$$

satisfying

$$L_1\left[C_1 + C_2\exp(\eta) + C_3\exp(-\eta)\right] = 0 \tag{27}$$

$$L_2\left[C_4\exp(\eta) + C_5\exp(-\eta)\right] = 0 \tag{28}$$

and C_i (i = 1, 2…5) are arbitrary constants. From eqs. (9)-(12), the non-linear operators N_f, N_g, N_θ, and N_ϕ, are defined by the following expressions:

$$N_f[f(\eta,p), g(\eta,p)] = \frac{\partial^3 f(\eta,p)}{\partial\eta^3} - \left(\frac{\partial f(\eta,p)}{\partial\eta}\right)^2 - (\varepsilon + M^2)\frac{\partial f(\eta,p)}{\partial\eta} + \\ + \left[f(\eta,p) + g(\eta,p)\right]\frac{\partial^2 f(\eta,p)}{\partial\eta^2} \tag{29}$$

$$N_g[f(\eta,p), g(\eta,p)] = \frac{\partial^3 g(\eta,p)}{\partial\eta^3} - \left(\frac{\partial g(\eta,p)}{\partial\eta}\right)^2 - (\varepsilon + M^2)\frac{\partial f(\eta,p)}{\partial\eta} + \\ + \left[f(\eta,p) + g(\eta,p)\right]\frac{\partial^2 g(\eta,p)}{\partial n^2} \tag{30}$$

$$N_\theta[\widehat{\theta}(\eta,p), f(\eta,p), g(\eta,p)] = \frac{\partial^2\widehat{\theta}(\eta,p)}{\partial\eta^2} + \Pr[\,\widehat{f}(\eta,p) + g(\eta,p)]\frac{\partial\widehat{\theta}(\eta,p)}{\partial\eta} + \\ + \Pr\left[\beta - r f(\eta,p) - sg(\eta,p)\right]\widehat{\theta}(\eta,p) \tag{31}$$

$$N_\phi[\widehat{\phi}(\eta,p) f(\eta,p) g(\eta,p] = \frac{\partial^2\widehat{\phi}(\eta,p)}{\partial\eta^2} + \Pr[f(\eta,p) + g(\eta,p)\frac{\partial\widehat{\phi}(\eta,p)}{\partial\eta} + \\ + \Pr\left[\beta - r f(\eta,p) - sg(\eta,p)\right]\widehat{\phi}(\eta,p) \tag{32}$$

If $p(\in[0,1])$ is the embedding parameter and $\hbar_f$, $\hbar_g$, $\hbar_\theta$, and $\hbar_\phi$ are the non-zero auxiliary parameters, respectively, the zeroth-order deformation problems are:

$$(1-p)L_1[\hat{f}(\eta,p)-f_0(\eta)] = p\hbar_f N_f[f(\eta,p)g(\eta,p)] \tag{33}$$

$$(1-p)L_1[g(\eta,p)-g_0(\eta)] = p\hbar_g N_g[g(\eta,p), f(\eta,p)] \tag{34}$$

$$(1-p)L_2[\hat{\theta}(\eta,p)-\theta(\eta)] = p\hbar_\theta N_\theta[\hat{\theta}(\eta,p), f(\eta,p)g(\eta,p)] \tag{35}$$

$$(1-p)L_2[\hat{\phi}(\eta,p)-\phi_0(\eta)] = p\hbar_\phi N_\phi[\hat{\phi}(\eta,p), g(\eta,p), f(\eta,p)] \tag{36}$$

$$f(0,p)=0,\ \left.\frac{\partial f(\eta,p)}{\partial\eta}\right|_{\eta=0}=1,\ g(0,p)=0,\ \left.\frac{\partial g(\eta,p)}{\partial\eta}\right|_{\eta=0}=\alpha,\ \hat{\theta}(\eta,p)=1,\ \left.\frac{\partial\hat{\phi}(\eta,p)}{\partial\eta}\right|_{\eta=0}=-1 \tag{37}$$

$$\left.\frac{\partial f(\eta,p)}{\partial\eta}\right|_{\eta=+\infty}=0,\quad \left.\frac{\partial g(\eta,p)}{\partial\eta}\right|_{\eta=+\infty}=0,\quad \hat{\theta}(\infty,p)=0,\quad \hat{\phi}(\infty,p)=0 \tag{38}$$

Note that for p = 0 and p = 1, the zeroth-order deformation eqs. (33)-(36) have the following solutions:

$$f(\eta,0)=f_0(\eta),\quad f(\eta,1)=f(\eta) \tag{39}$$

$$g(\eta,0)=g_0(\eta),\quad g(\eta,1)=g(\eta) \tag{40}$$

$$\hat{\theta}(\eta,0)=\theta_0(\eta),\quad \hat{\theta}(\eta,1)=\theta(\eta) \tag{41}$$

$$\hat{\phi}(\eta,0)=\phi_0(\eta),\quad \hat{\phi}(\eta,1)=\phi(\eta) \tag{42}$$

By increasing p from 0 to 1 , $f(\eta,p)$, $g(\eta,p)$, $\hat{\theta}(\eta,p)$, and $\hat{\phi}(\eta,p)$ vary from $f_0(\eta)$, $g_0(\eta)$, $\theta_0(\eta)$, and $\phi_0(\eta)$ to the solutions $f(\eta)$, $g(\eta)$, $\theta(\eta)$, and $\phi(\eta)$ of the original eqs. (9)-(12). Due to Taylor's theorem and above expressions, the power series are:

$$f(\eta,p)=f_0(\eta)+\sum_{m=1}^{\infty}f_\mathrm{m}(\eta)\,p^\mathrm{m},\quad f_\mathrm{m}(\eta)=\left.\frac{1}{m!}\frac{\partial^\mathrm{m} f(\eta,p)}{\partial p^\mathrm{m}}\right|_{p=0} \tag{43}$$

$$g(\eta,p)=g_0(\eta)+\sum_{m=1}^{\infty}g_\mathrm{m}(\eta)\,p^\mathrm{m},\quad g_\mathrm{m}(\eta)=\left.\frac{1}{m!}\frac{\partial^\mathrm{m} g(\eta,p)}{\partial p^\mathrm{m}}\right|_{p=0} \tag{44}$$

$$\hat{\theta}(\eta,p)=\theta_0(\eta)+\sum_{m=1}^{\infty}\theta_\mathrm{m}(\eta)\,p^\mathrm{m},\quad \theta_\mathrm{m}(\eta)=\left.\frac{1}{m!}\frac{\partial^\mathrm{m}\hat{\theta}(\eta,p)}{\partial p^\mathrm{m}}\right|_{p=0} \tag{45}$$

$$\widehat{\phi}(\eta,p)=\phi_0(\eta)+\sum_{m=1}^{\infty}\phi_{\mathrm{m}}(\eta)\,p^{\mathrm{m}},\quad \phi_{\mathrm{m}}(\eta)=\frac{1}{m!}\frac{\partial^{\mathrm{m}}\widehat{\phi}(\eta,p)}{\partial p^{\mathrm{m}}}\bigg|_{p=0} \tag{46}$$

Obviously eqs. (33)-(36) contain four non-zero auxiliary parameters $\hbar_{\mathrm{f}}$, $\hbar_{\mathrm{g}}$, $\hbar_{\theta}$, and $\hbar_{\phi}$. Assuming that $\hbar_{\mathrm{f}}$, $\hbar_{\mathrm{g}}$, $\hbar_{\theta}$, and $\hbar_{\phi}$ are chosen in such a way that the series in eqs. (43) and (46) are convergent at p = 1. Employing eqs. (39)-(42) we get:

$$f(\eta)=f_0(\eta)+\sum_{m=1}^{\infty}f_{\mathrm{m}}(\eta) \tag{47}$$

$$g(\eta)=g_0(\eta)+\sum_{m=1}^{\infty}g_{\mathrm{m}}(\eta) \tag{48}$$

$$\theta(\eta)=\theta_0(\eta)+\sum_{m=1}^{\infty}\theta_{\mathrm{m}}(\eta) \tag{49}$$

$$\phi(\eta)=\phi_0(\eta)+\sum_{m=1}^{\infty}\phi_{\mathrm{m}}(\eta) \tag{50}$$

For m^{th} order deformation problems, we differentiate eqs. (29)-(32) m times with respect to p, set p = 0 and get after dividing by m! the following:

$$L_1[f_{\mathrm{m}}(\eta)-\chi_{\mathrm{m}}f_{\mathrm{m-1}}(\eta)]=\hbar_{\mathrm{f}}R_{\mathrm{m}}^{\mathrm{f}}(\eta) \tag{51}$$

$$L_1[g_{\mathrm{m}}(\eta)-\chi_{\mathrm{m}}g_{\mathrm{m-1}}(\eta)]=\hbar_{\mathrm{g}}R_{\mathrm{m}}^{\mathrm{g}}(\eta) \tag{52}$$

$$L_2[\theta_{\mathrm{m}}(\eta)-\chi_{\mathrm{m}}\theta_{\mathrm{m-1}}(\eta)]=\hbar_{\theta}R_{\mathrm{m}}^{\theta}(\eta) \tag{53}$$

$$L_2[\phi_{\mathrm{m}}(\eta)-\chi_{\mathrm{m}}\phi_{\mathrm{m-1}}(\eta)]=\hbar_{\phi}R_{\mathrm{m}}^{\phi}(\eta) \tag{54}$$

$$f_{\mathrm{m}}(0)=f'_{\mathrm{m}}(0)=g_{\mathrm{m}}(0)=g'_{\mathrm{m}}(0)=\theta_{\mathrm{m}}(0)=\phi'_{\mathrm{m}}(0)=0 \tag{55}$$

$$f'_{\mathrm{m}}(\infty)=g'_{\mathrm{m}}(\infty)=\theta_{\mathrm{m}}(\infty)=\phi_{\mathrm{m}}(\infty)=0 \tag{56}$$

where

$$R_{\mathrm{m}}^{\mathrm{f}}(\eta)=f'''_{\mathrm{m-1}}(\eta)-(\varepsilon+M^2)\,f'_{\mathrm{m-1}}+\sum_{k=0}^{m-1}[(f_{\mathrm{m-1-k}}+g_{\mathrm{m-1-k}})f''_{\mathrm{k}}-f'_{\mathrm{m-1-k}}f'_{\mathrm{k}}]$$

$$R_{\mathrm{m}}^{\mathrm{g}}(\eta)=g'''_{\mathrm{m-1}}(\eta)-(\varepsilon+M^2)\,g'_{\mathrm{m-1}}+\sum_{k=0}^{m-1}[(f_{\mathrm{m-1-k}}+g_{\mathrm{m-1-k}})g''_{\mathrm{k}}-g'_{\mathrm{m-1-k}}g'_{\mathrm{k}}]$$

$$R_{\mathrm{m}}^{\theta}(\eta)=\theta''_{\mathrm{m-1}}(\eta)+\Pr\beta\theta_{\mathrm{m-1}}+\Pr\sum_{k=0}^{m-1}[(f_{\mathrm{m-1-k}}+g_{\mathrm{m-1-k}})\theta'_k-(rf'_{\mathrm{m-1-k}}+sg'_{\mathrm{m-1-k}})\theta_k]$$

$$R_{\mathrm{m}}^{\phi}(\eta)=\phi''_{\mathrm{m-1}}(\eta)+\Pr\beta\phi_{\mathrm{m-1}}+\Pr\sum_{k=0}^{m-1}[(f_{\mathrm{m-1-k}}+g_{\mathrm{m-1-k}})\phi'_{\mathrm{k}}-(rf'_{\mathrm{m-1-k}}+sg'_{\mathrm{m-1-k}})\phi_{\mathrm{k}}]$$

$$\chi_{\mathrm{m}}=\begin{vmatrix}0, & m\le 1\\ 1, & m>1\end{vmatrix} \tag{57}$$

Equations (51) to (56) have the general solutions in the forms:

$$f_{\mathrm{m}}(\eta)=f_{\mathrm{m}}^{?}(\eta)+C_1+C_2\exp(\eta)+C_3\exp(-\eta) \tag{58}$$

$$g_{\mathrm{m}}(\eta)=g_{\mathrm{m}}^{?}(\eta)+C_4+C_5\exp(\eta)+C_6\exp(-\eta) \tag{59}$$

$$\theta_{\mathrm{m}}(\eta)=\theta_{\mathrm{m}}^{?}(\eta)+C_7\exp(\eta)+C_8\exp(-\eta) \tag{60}$$

$$\phi_{\mathrm{m}}(\eta)=\phi_{\mathrm{m}}^{?}(\eta)+C_9\exp(\eta)+C_{10}\exp(-\eta) \tag{61}$$

where $f_{\mathrm{m}}^{?}(\eta)$, $g_{\mathrm{m}}^{?}(\eta)$, $\theta_{\mathrm{m}}^{?}(\eta)$, and $\phi_{\mathrm{m}}^{?}(\eta)$ satisfy the special solutions of eqs. (51)-(54) and the integral constants C_i, (i = 1-10) are determined by the boundary conditions (55) and (56):

$$C_2=0,\quad C_3=\left.\frac{\partial f_{\mathrm{m}}^{?}(\eta)}{\partial\eta}\right|_{\eta=0},\quad C_1=-C_3-f_{\mathrm{m}}^{?}(0) \tag{62}$$

$$C_5=0,\quad C_6=\left.\frac{\partial g_{\mathrm{m}}^{?}(\eta)}{\partial\eta}\right|_{\eta=0},\quad C_4=-C_6-f_{\mathrm{m}}^{?}(0) \tag{63}$$

$$C_7=0,\quad C_8=-\theta_{\mathrm{m}}^{?}(0) \tag{64}$$

$$C_9=0,\quad C_{10}=-\phi_{\mathrm{m}}^{?}(0) \tag{64}$$

Now it is easy to solve the system of linear non-homogeneous eqs. (51)-(54) by using Mathematica one after the other in the order m = 1, 2, 3…

Convergence of the HAM solutions

As pointed out by Liu *et al.* [17] that the solutions series given by the eqs. (47)-(50) contains the auxiliary parameters $\hbar_{\mathrm{f}}$, $\hbar_{\mathrm{g}}$, $\hbar_\theta$, and $\hbar_\phi$. The convergence and rate of approximation of the homotopy analysis solutions strongly depend upon $\hbar_{\mathrm{f}}$, $\hbar_{\mathrm{g}}$, $\hbar_\theta$, and $\hbar_\phi$. For the convergence of these solutions, one can choose the proper values of $\hbar_{\mathrm{f}}$, $\hbar_{\mathrm{g}}$, $\hbar_\theta$, and $\hbar_\phi$ by plotting the so-called $\hbar$-curves. Therefore, the $\hbar$-curves of f'' (0), g'' (0), $\theta'(0)$, and $\phi''(0)$ are shown for 15th order of approximation in fig. 1. For simplicity we put $\hbar_{\mathrm{f}}=\hbar_{\mathrm{g}}=\hbar_\theta=\hbar_\phi=\hbar$, and thus from fig. 1 we see that the range for the admissible values of for f'' (0) $\hbar g''(0)$, θ' (0), and ϕ'' (0) is $-0.85\le\hbar\le-0.3$. Our analysis indicates that the solutions (47)-(50) converge in the whole region of η, when $\hbar$ = – – 0.6.

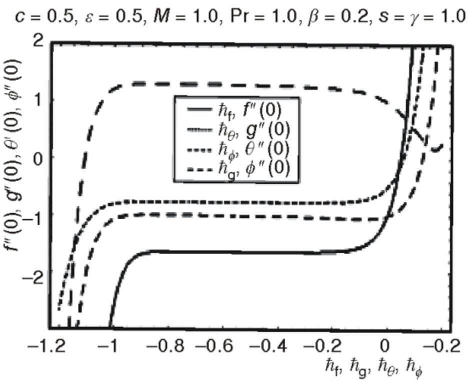

Figure 1. The $\hbar$-curves of $f''(0)$, $g''(0)$, $\theta'(0)$, and $\phi''(0)$ at the 15th order of approximation

Results and discussion

We have obtained the velocity and temperature profiles f', g', θ and ϕ in the form of series given in eqs. (47)-(50). In order to see the influence of the salient features of the involved parameters on the velocity and temperature profiles, we plot figs. (2-9).

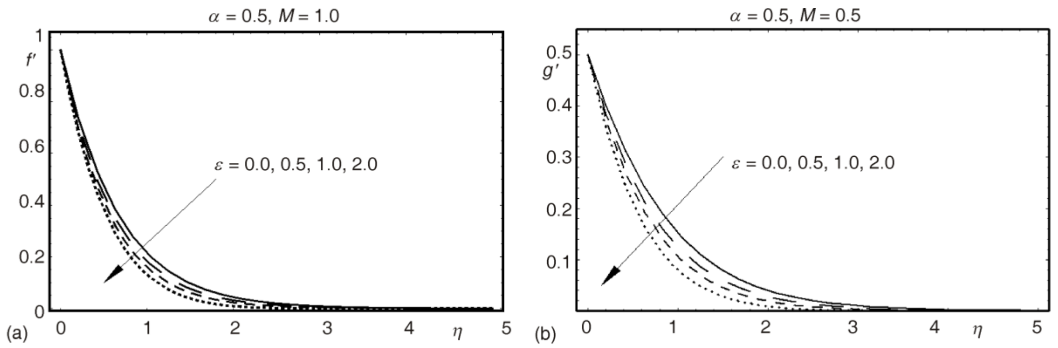

Figure 2. Velocity profiles $f'(\eta)$ and $g'(\eta)$ *vs.* η for different values of porosity parameter ε with α = 0.5 and M = 0.5

Figure 2 shows the effects of porosity parameter ε on the velocity components f' and g' when α = 0.5 and M = 0.5. It is noted that both the velocity components f' and g' are decreased by increasing the values of the porosity parameter ε. The boundary layer thickness also decreases for large values of ε. Figure 3 gives the variation of the velocity f' and g' for different values of the magnetic parameter M by keeping α = 0.5 and ε = 0.5 fixed. It can be seen from this figure that the influence of the magnetic field causes to reduce the boundary layer thickness. As expected, the magnetic force is a resistance to the flow, hence reduces the velocity magnitude of f' and g', respectively. The dimensionless velocity components f' and g' presented in fig. 4 give the influences of the stretching ratio α. It is observed from fig. 4(a) that the velocity f' decreases with increasing values of the stretching ratio α, while the velocity g' increases by increasing the values of α as in fig. 4(b).

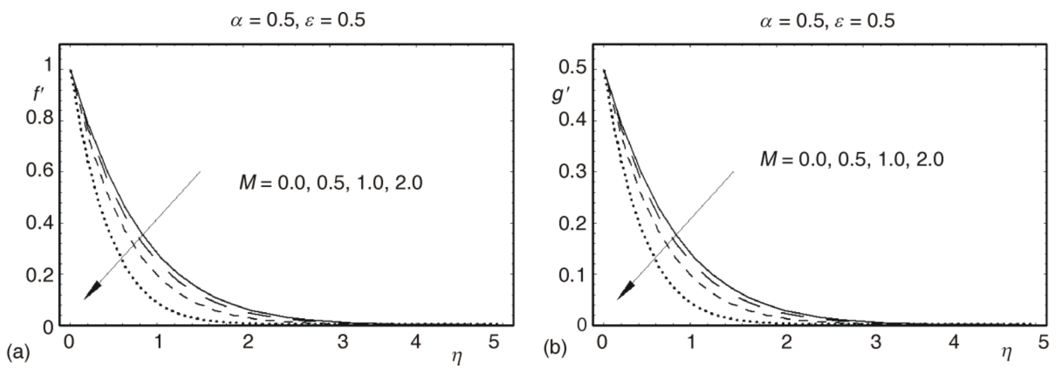

Figure 3. Velocity profiles $f'(\eta)$ and $g'(\eta)$ *vs.* η for different values of magnetic parameter M with α = 0.5 and ε = 0.5

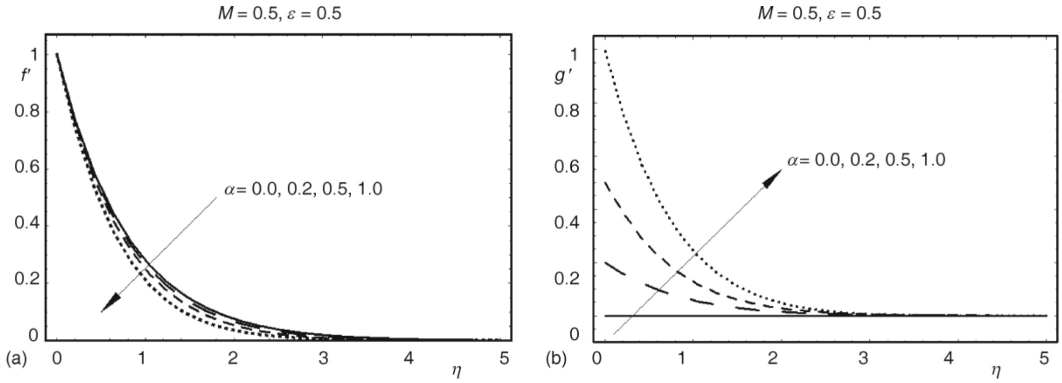

Figure 4. Velocity profiles $f'(\eta)$ and $g'(\eta)$ *vs.* η for different values of stretching ratio *a* with M = 0.5, ε = 0.5

Figure 5 shows the effects of the magnetic parameter M on the dimensionless temperature profiles θ and ϕ by keeping α = 0.5 and ε = 0.5 fixed. The temperature profiles increase with increasing the values of the magnetic parameter M in both the cases of the PST and PHF, respectively. It is also noted that this increment is slightly larger in case of PHF.

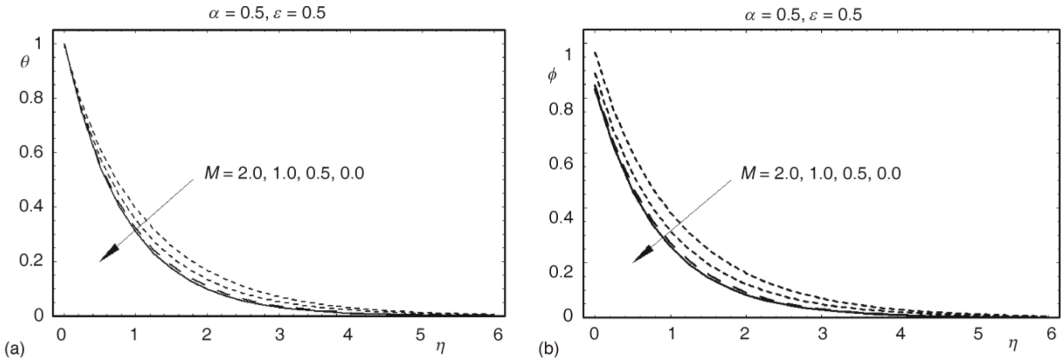

Figure 5. Temperature profiles $\theta(\eta)$ and $\phi(\eta)$ *vs.* η for different values of magnetic parameter M with α = 0.5 and ε = 0.5

Figure 6 elucidates the influences of the stretching ratio α on the temperature profiles θ and ϕ for the case of (r = s = 1) and Pr = 1 with ε = 0.5 and M = 0.5. It is observed that the temperature profile decreases with increasing values of the stretching ratio α in both the cases of the PST and PHF. It is also observed that the thermal boundary layer is decreased for large values of the stretching ratio α. It is further noted that these results are in qualitatively similar with the temperature profiles shown by Liu *et al.* [17] in the presence of the magnetic field and porous medium. Figure 7 shows the effects of the power indices r on the temperatures θ and ϕ in case of s = 0 with M = 0.5 and ε = 0.5 keeping fixed. It is noted that as we increase the values of r both the temperature profiles and the thermal boundary layer thickness are decreased. From fig. 7, it can also be seen that the temperature rises above the sheet temperature for r = –3 and r = –2 and than decreases as the distance in the x-direction from the origin increases and the heat flux is therefore directed from the fluid to the sheet, rather

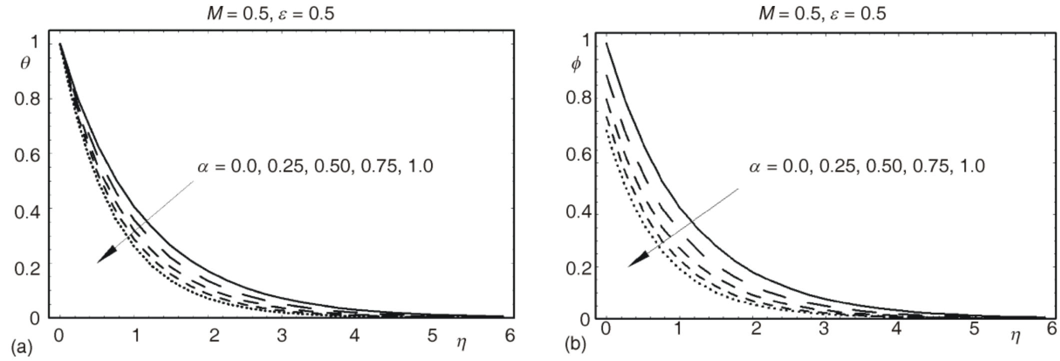

Figure 6. Temperature profiles $\theta(\eta)$ and $\phi(\eta)$ *vs.* η for different values of stretching ratio α with M = 0.5 and ε = 0.5

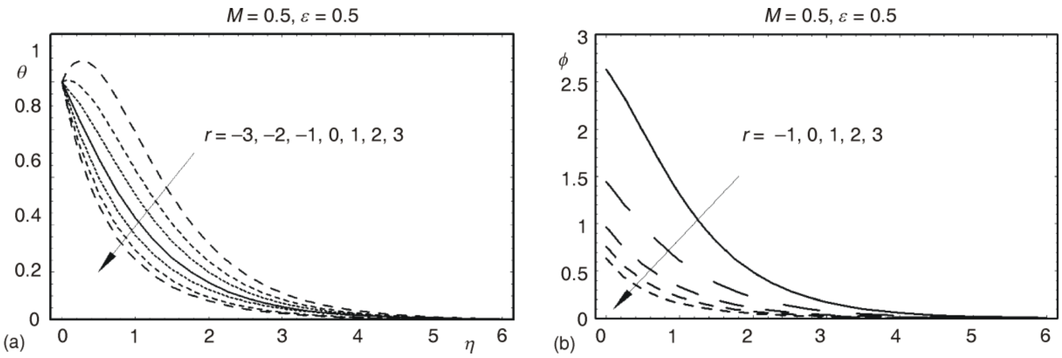

Figure 7. Temperature profiles $\theta(\eta)$ and $\phi(\eta)$ *vs.* η for different values *r* with M = 0.5, ε = 0.5, and α = 0.5

than in the common direction from the sheet to the fluid as for $r > -1$ as mentioned in Liu *et al*. [17] in the presence of the magnetic field and porous medium, but the change in temperature is smaller in case of $M = \varepsilon \neq 0$. Figure 8 gives the influences of the power indices *s* on the temperature when the sheet temperature is uniform in the x-direction ($r = 0$)

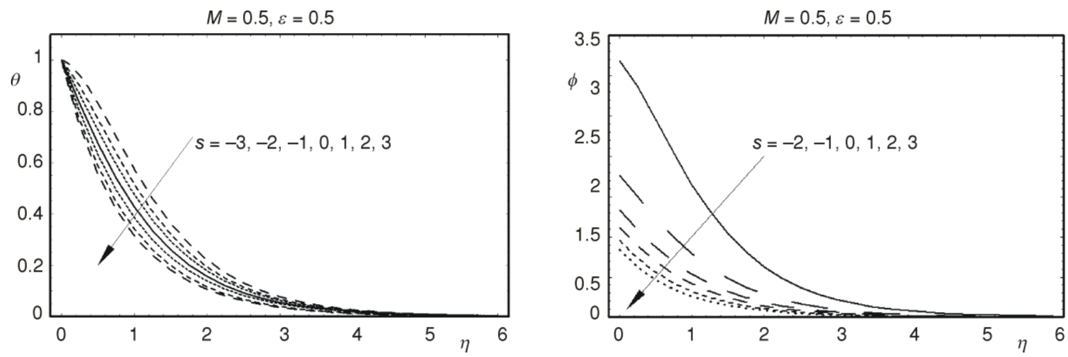

Figure 8. Temperature profiles $\theta(\eta)$ and $\phi(\eta)$ *vs.* η for different values *s* with M = 0.5, ε = 0.5, and α = 0.5

with M = 0.5, and ε = 0.5 keeping fixed. The temperature and the thermal boundary layer thickness are decreased as we increase the values of s from s = –3 to s = 3. Figure 9. shows the effects of the heat source/sink parameter β on the temperatures θ and ϕ with Pr = 1, r = s = 1, M = 0.5, α = 0.5, and ε = 0.5. As expected, the temperature increases with increasing heat source β > 0 and decreases in the case of heat sink β < 0 in both cases of PST and PHF.

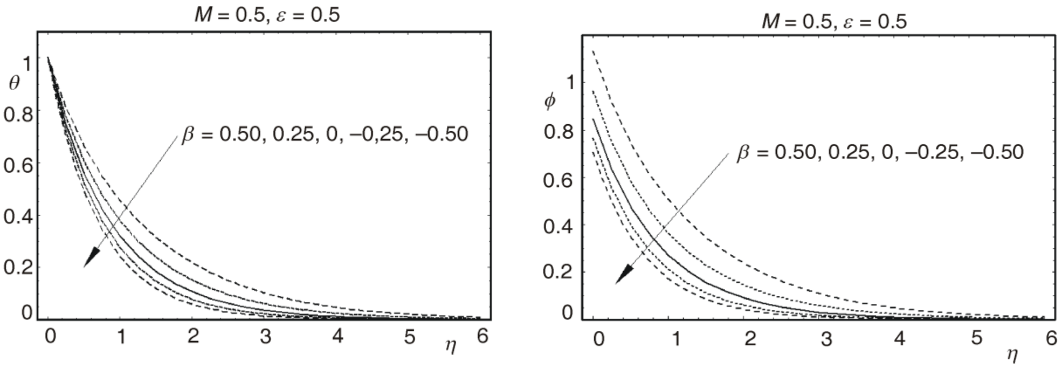

Figure 9. Temperature profiles $\theta(\eta)$ and $\phi(\eta)$ *vs.* η for different values β with M = 0.5, ε = 0.5, and α = 0.5

Table 1 shows the numerical values of $f''(0)$, $g''(0)$, $f(\infty)$, and $g(\infty)$, for hydrodynamical problem in absence of magnetic field M = 1 and porous medium ε = 0. It is noted that the magnitudes of the shear stresses at the wall $f''(0)$ and $g''(0)$, in the x-and y-directions are increased by increasing the values of the stretching ratio α. It is further noted that the present results of HAM are compared with the data given by Wang [14] and Liu *et al*. [17] and found in excellent agreement.

Table 1. Numerical values of $f''(0)$, $g''(0)$, $f(\infty)$, and $g(\infty)$ when ε = 0 and M = 0

		$f''(0)$	$g''(0)$	$f(\infty)$	$g(\infty)$
Wang [14]	α = 0.0	–1	0	1	0
Lui *et al.* [17]		–1	0	1	0
HAM		–1	0	1	0
Wang [14]	α = 0.25	–1.048813	–0.194564	0.907075	0.257986
Lui *et al.* [17]		–1.048813	–0.194565	0.907067	0.257966
HAM		–1.048811	–0.194564	0.907046	0.257993
Wang [14]	α = 0.50	–1.093097	–0.465205	0.842360	0.451671
Lui *et al.* [17]		–1.093096	–0.465206	0.842361	0.451663
HAM		–1.093095	–0.465205	0.842386	0.451677
Wang [14]	α = 0.75	–1.134485	–0.794622	0.792308	0.612049
Lui *et al.* [17]		–1.134486	–0.794619	0.792293	0.612128
HAM		–1.134486	–0.794618	0.792302	0.612135
Wang [14]	α = 1.0	–1.173720	–1.173720	0.751527	0.751527
Lui *et al.* [17]		–1.173721	–1.173721	0.751494	0.751494
HAM		–1.173721	–1.173721	0.751497	0.751497

Table 2 is made to give the numerical values of $f''(0)$, $g''(0)$, $f(\infty)$, and $g(\infty)$ and in the presence of the magnetic field M □ 0 and porous medium ε □ 0. It is observed that the magnitudes of the shear stresses at the wall $f''(0)$ and $g''(0)$ are larger in case of (M □0 and ε □ □0) as compared to the case $M = \varepsilon = 0$. Table 3 shows the values of the temperature gradient at the surface $\theta'(0)$ for different values of r and s with $\beta = 0$ and Pr = 1 in case of $M = \varepsilon = 0$. It is found that the temperature gradient at the surface $\theta'(0)$ becomes positive and decreases for $r = -2$ and $s = 0$ and negative for $r = 0$ and $s = -2$. It is also noted that the present results obtained by HAM has a good agreement with the numerical results given by Liu *et al*. [17]. Table 4 gives the values of the temperature gradient at the surface $\theta'(0)$ for different values of r and s with $\beta = 0$ and Pr = 1 in the presence of the magnetic field $M = 5$ and porosity parameter $\varepsilon = 0.2$. It is observed that the temperature gradient at the surface $\theta'(0)$ has the same behavior in case of $M = 0.5$ and $\varepsilon = 0.2$, but its magnitude is smaller in this case when compared with the case of $M = \varepsilon = 0$. Table 5 gives the numerical values of the temperature gradient

Table 2. Numerical values of $f''(0)$, $g''(0)$, $f(\infty)$, and $g(\infty)$ when $\varepsilon = 0.5$ and $M = 0.5$

	$f''(0)$	$g''(0)$	$f(\infty)$	$g(\infty)$
$\alpha = 0.0$	–1.204159	0	0.830455	0
$\alpha = 0.25$	–1.242674	–0.255757	0.778887	0.212809
$\alpha = 0.50$	–1.279160	–0.571163	0.737905	0.388412
$\alpha = 0.75$	–1.314085	–0.937135	0.703896	0.540092
$\alpha = 1.0$	–1.347728	–1.347728	0.674873	0.674873

Table 3. Temperature gradient at the surface $\theta(0)$ for selected values of r and s with $\beta = 0$, $\varepsilon = 0 = M$, and Pr = 1

		$r = 0, s = 0$	$r = -2, s = 0$	$r = 2, s = 0$	$r = 0, s = -2$	$r = 0, s = 2$
Ref. [17]	$\alpha = 0.25$	–0.665933	0.554512	–1.364890	–0413111	–0.883125
Present		–0.665927	0.554573	–1.364890	–0413101	–0.883123
Ref. [17]	$\alpha = 0.50$	–0.735334	0.308578	–1.395356	–0.263381	–1.106491
Present		–0.735333	0.308590	–1.395357	–0.263376	–1.106500
Ref. [17]	$\alpha = 0.75$	–0.796472	0.135471	–1.425038	–0.126679	–1.292003
Present		–0.796470	0.135470	–1.425037	–0.126680	–1.292010

Table 4. Temperature gradient at the surface $\theta'(0)$ for selected values of r and s with $\beta = 0$, $\varepsilon = 0.2$, $M = 0.5$, and Pr = 1

	$r = 0, s = 0$	$r = -2, s = 0$	$r = 2, s = 0$	$r = 0, s = -2$	$r = 0, s = 2$
$\alpha = 0.25$	–0.625146	0.500062	–1.311314	–0.388527	–0.832651
$\alpha = 0.50$	–0.696653	0.287065	–1.345355	–0.249419	–1.057183
$\alpha = 0.75$	–0.759970	0.128083	–1.378118	–0.120535	–1.245219

Table 5. Temperature gradient at the surface $\theta'(0)$ and $\phi(0)$ for selected values of Pr and β with ε = 0, M = 0, r = 1, s = 1, and α = 0.5

		$\theta'(0)$ for PST			$\phi(0)$ for PHF		
		β = –0.2	β = 0	β = 0.2	β = –0.2	β = 0	β = 0.2
Ref. [17]	Pr = 1	–1.348064	–1.255781	–1.148932	0.741805	0.796317	0.870355
Present		–1.348064	–1.255780	–1.148934	0.741808	0.796318	0.870372
Ref. [17]	Pr = 5	–3.330392	–3.170979	–3.002380	0.300265	0.315360	0.333069
Present		–3.330394	–3.170981	–3.002384	0.3002657	0.315363	0.333071
Ref. [17]	Pr = 10	–4.812149	–4.597141	–4.371512	0.207807	0.217527	0.228754
Present		–4.812151	–4.597143	–4371516	0.207809	0.217529	0.228756

at the surface $\theta'(0)$ and $\phi(0)$ for different values of Pr and β with α = 0.5, s = 1, r = 1, and M = = ε = 0. The magnitude of the temperature gradient at the surface $\theta'(0)$ increases by increasing the values of Pr and $-\theta(0)$ reduces with increasing values of β. It is also noted from this table that in case of PHF at the sheet, a heat source (sink) tends to reduce the sheet temperature $\phi(0)$. Table 6 shows the numerical values of the temperature gradient at the surface $\theta'(0)$ and $\phi(0)$ for different values of Pr and β with α = 0.5, s = 1, r = 1 in case of M = = 5 and ε = 0.2. It is noted that the magnitude of the temperature gradient at the surface $\theta'(0)$ is smaller, whereas the sheet temperature $\phi(0)$ in case of prescribed heat flux at the sheet is larger quantitatively in the presence of magnetic field M = 0.5 and porosity parameter ε = 0.2.

Table 6. Temperature gradient at the surface $\theta'(0)$ and $\phi(0)$ for selected values of Pr and β with ε = 0.2, M = 0.5, r = 1.0, s = 1, and α = 0.5

	$\theta'(0)$ for PST			$\phi(0)$ for PHF		
	β = –0.2	β = 0	β = 0.2	β = –0.2	β = 0	β = 0.2
Pr = 1	–1.306568	–1.205991	–1.082238	0.765364	0.829193	0.923981
Pr = 5	–3.234749	–3.094872	–3.000234	0.304281	0.320426	0.337240
Pr = 10	–4.702361	–4.436862	–4.315217	0.210176	0.226381	0.231123

Conclusions

The MHD 3-D flow and heat transfer characteristics of a viscous fluid due to a bidirectional stretching sheet through a porous medium is investigated in this paper. For the heat transfer analysis the heating processes of (1) the PST and (2) PHF are taken into account. The influence of the various parameters of interest are analyzed through the similarity solution of the governing equations. The main findings of the present study are:

- boundary layer thickness is a decreasing function of porosity parameter and the Hartman number,
- thermal boundary layer increases by increasing the values of porosity parameter and applied magnetic field,
- both temperature and thermal boundary layer thickness are decreased when the Prandtl number increases, and
- the heat flux through the wall decreases by an increase in the internal heat parameter β.

Nomenclature

A, B – positive constants
a, b – constants stretching rates, [s^{-1}]
$\vec{B}_0$ – magnetic field, [T]
c_p – specific heat at constant pressure, [$Jkg^{-1}K^{-1}$]
f, g – real functions
$\hbar_f$, $\hbar_g$, $\hbar_\theta$, $\hbar_\phi$ – non-zero auxiliary parameters
k – permeability of the porous medium, [m^2]
k_1 – thermal diffusivity, [ms^{-1}]
L_1, L_2 – auxiliary linear operators
M^2 – Hartman number, ($= \sigma \vec{B}_0^2/a\rho$)
N_f, N_g, N_θ, N_ϕ – non-linear operators
p – the embedding parameter
Pr – Prandtl number, ($=\nu/k_1$), [–]
q – heat source or sink, [W]
r, s – power indices, [m]
Re – Reynolds number, [–]
T – temperature of the fluid, [K]
T_w – temperature at the surface of the plate, [K]
T_∞ – temperature of the ambient fluid, [K]
u, v, w – velocities in x-, y-, and z-direction, [ms^{-1}]
x, y, z – spatial co-ordinates, [m]

Greeks symbols

α – the stretching ratio (= b/a), [–]
β – diemnsionless internal heat parameter ($= q/\rho a c_p$), [–]
ε – dimensionless porosity parameter ($= \phi_1/\rho a k$), [–]
η – similarity variable, [–]
θ – dimensionless temperature, $(T - T_\infty)/(T_w - T_\infty)$, [–]
λ – thermal conductivity of the fluid, [$Wm^{-1}K^{-1}$]
μ – dynamic viscosity, [$kgm^{-1}s^{-1}$]
ν – kinematic viscosity, [m^2s^{-1}]
ρ – fluid density, [kgm^{-3}]
ϕ – dimensionless temperature for PHF, [–]
ϕ_1 – porosity of the porous medium
σ – electrical conductivity of the fluid, [sm^{-1}]

Subscripts

i – arbitrary constants
f, g, θ, ϕ – indications for the functions f, g, θ, ϕ
p – constant pressure
w – surface conditions
1 – porous medium
∞ – conditions far away from the surface

Acronyms

PHF – presscribed surface heat flux
PST – prescribed surface temperature
HAM – homotopy analysis method

References

[1] Sakiadis, B. C., Boundary Layer behavior on Continuous Solid Surface, I. Boundary Layer Equation for Two-Dimensional and Axisymmetric Flow, *AIChE J.*, *7* (1961), 1, pp. 26-28
[2] Sakiadis, B. C., Boundary Layer behavior on Continuous Solid Surface, II. Boundary Layer Equations on Continuous Solid Surface, *AIChE J.*, *7* (1961), 2, pp. 221-225
[3] McCormack, P. D., Crane, L., Physical Fluid Dynamics, Academic Press, New York, USA, 1973
[4] Gupta, P. S., Gupta, A. S., Heat and Mass Transfer on a Stretching Sheet with Suction or Blowing, *Can. J. Chem. Eng., 55* (1977), 6, pp. 744-756
[5] Cortell, R., Similarity Solutions for Flow and Heat Transfer in a Viscoelastic Fluid over a Stretching Sheet, *Int. J. Non-Linear Mech., 29* (1994), 2, pp. 155-161
[6] Vleggaar, J., Laminar Boundary Layer behaviour on Continuous Accelerating Surface, *Chem. Eng. Sci., 32* (1977), 12, pp. 1517-1525
[7] Dutta, B. K., Roy, P., Gupta. A. S., Temperature Field in a Flow over a Stretching Sheet with Uniform Heat Flux, *Int. Commun*. *Heat Mass Transfer, 12* (1985), 1, pp.89-94
[8] Magyari, E., Keller, B., Exact Solutions for Self-Similar Boundary-Layer Flows Induced by Permeable Stretching Walls, *Eur. J. Mech.B-Fluids, 19* (2000), 1, pp. 109-122
[9] Crane, L., Flow Past a Stretching Plate, *Z. Angew Math. Phys., 4* (1970), 21, pp. 645-647
[10] Banks, W. H. H., Similarity Solutions of the Boundary Layer Equations for a Stretching Wall, *J. Mech Theor. Appl., 2* (1983), 3, pp. 375-392
[11] Ali, M. E., Heat Transfer Characteristics of a Continuous Stretching Surface, *Heat and Mass Transfer, 29* (1994), 4, pp. 227-234
[12] Hayat, T., Sajid, M., Analytic Solution for Axisymmetric Flow and Heat Transfer of a Second Grade Fluid Past a Stretching Sheet, *Int. J. Heat Mass Transfer, 50* (2007), 1-2, pp. 75-84

[13] Kumar, H., Radiation Heat Transfer with Hydromagnetic Flow and Viscous Dissipation over a Stetching Surface in the Presence of Variable Heat Flux, *Thermal Science, 13* (2009), 2, pp. 163-169
[14] Wang, C. Y., The Three Dimensional Flow Due to Stretching Surface, *Phys. Fluids, 27* (1984), pp. 1915-1917
[15] Laha, M. K., Gupta, P. S., Gupta, A. S., Heat Transfer Characteristics of the Flow of an Incompressible Viscous Fluid over a Stretching Sheet, *Heat and Mas Transfer, 24* (1998), 3, pp. 151-153
[16] Ariel, P. D., Generalized Three Dimensional Flow Due to Stretching Surface, *Z. Angew. Math. Mech, 83* (2003), 12, pp. 844-852
[17] Liu, I.-C., Andersson, H. I., Heat Transfer over a Bidirectional Stretching Sheet with Variable Thermal Conditions, *Int. J. Heat Mass Transfer, 51* (2008), 15-16, pp. 4018-4024
[18] Abdullah, I. A., Analytic Solution of Heat and Mass Transfer over a Permeable Stretching Plate Affected by Chemical Reaction, Internal Heating, Dufour-Soret Effect and Hall Effect, *Thermal Science, 13* (2009), 2, pp. 183-197
[19] Liao, S. J., Beyond Perturbation: Introduction to Homotopy Analysis Method, Chapman & Hall, Boca Raton, Fla., USA, 2003
[20] Liao, S. J., On the Homotopy Analysis Method for Nonlinear Problems, *Appl. Math. Comput., 147* (2004), 2, pp. 499-513
[21] Sajid, M., Hayat, T., Asghar, S., On the Analytic Solution of the Steady Flow of a Fourth Grade Fluid, *Phys. Lett. A, 355* (2008), 1, pp. 18-24
[22] Abbas, Z., Sajid, M., Hayat, T., MHD Boundary Layer Flow of an Upper-Convected Maxwell Fluid in a Channel, *Theor. Comput. Fluid. Dyn., 20* (2006), 4, pp. 229-238
[23] Liao, S. J., A Uniformly Valid Analytic Solution of 2-D Viscous Flow Past a Semi-Infinite Flat Plate, *J. Fluid Mech., 385* (1999), 1, pp. 101-128
[24] Liao, S. J., Campo, A., Analytic Solutions of the Temperature Distribution in Blasius Viscous Flow Problems, *J. Fluid Mech., 453* (2002), pp. 411-425
[25] Cheng, J., Liao, S. J., Pop, I., Analytic Series Solution for Unsteady Mixed Convection Boundary Layer Flow Near the Stagnation Point on a Vertical Surface in a Porous Medium, *Transport in Porous Media, 61* (2005), 3, pp. 365-379
[26] Yang, C., Liao, S. J., On the Explicit Purely Analytic Solution of Von Karman Swirling Viscous Flow, *Comm. Non-linear Sci. Numer. Simm., 11* (2006), 1, pp. 83-93
[27] Abbasbandy, S., Homotopy Analysis Method for Heat Radiation Equations, *Int. Comm. Heat and Mass Transfer, 34* (2007), 3, pp. 380-387
[28] Hayat, T., Sajid, M., Ayub, M., A Note on Series Solution for Generalized Couette Flow, *Comm. Non-linear Sci. Numer. Simm., 12* (2007), 8, pp. 1481-1487

Paper submitted: September 26, 2010
Paper revised: January 20, 2011
Paper accepted: January 23, 2011